Molecular Dynamics Simulation of Liquid Water Confined inside Graphite Channels: Dielectric and Dynamical Properties

J. Martí,*,† G. Nagy,‡ E. Guàrdia,† and M. C. Gordillo§

Departament de Física i Enginyeria Nuclear, Universitat Politècnica de Catalunya, B5-206 Campus Nord., 08034 Barcelona, Catalonia, Spain, Materials Department, KFKI-Atomic Energy Research Institute, H-1525 Budapest, P.O. Box 49 Hungary, and Departamento de Sistemas Físicos, Químicos y Naturales, Facultad de Ciencias Experimentales, Universidad Pablo de Olavide. Ctra. de Utrera, Km. 1. Sevilla, Spain

Received: July 25, 2006; In Final Form: September 22, 2006

Electric and dielectric properties and microscopic dynamics of liquid water confined between graphite slabs are analyzed by means of molecular dynamics simulations for several graphite−graphite separations at ambient conditions. The electric potential across the interface shows oscillations due to water layering, and the overall potential drop is about −0.28 V. The total dielectric constant is larger than the corresponding value for the bulklike internal region of the system. This is mainly due to the preferential orientations of water nearest the graphite walls. Estimation of the capacitance of the system is reported, indicating large variations for the different adsorption layers. The main trend observed concerning water diffusion is 2-fold: on one hand, the overall diffusion of water is markedly smaller for the closest graphite−graphite separations, and on the other hand, water molecules diffuse in interfaces slightly slower than those in the bulklike internal areas. Molecular reorientational times are generally larger than those corresponding to those of unconstrained bulk water. The analysis of spectral densities revealed significant spectral shifts, compared to the bands in unconstrained water, in different frequency regions, and associated to confinement effects. These findings are important because of the scarce information available from experimental, theoretical, and computer simulation research into the dielectric and dynamical properties of confined water.

Introduction

Liquid−surface interactions are of central importance in a number of fields such as electrochemistry,[1,2] the physics and chemistry of corrosion,[3,4] heterogeneous catalysis of metals,[5,6] solar energy conversion,[7] or liquid transport of geological materials such as clays or rocks. In particular, liquid water suffers dramatic changes in its microscopic structure and dynamics as well as in its dielectric properties when it is placed near solid surfaces of any class (hydrophilic or hydrophobic). Liquid water in confined geometries has received great interest in recent years from both computer simulation and the experimental point of view. Pioneering[8,9] and recent computer simulation works[10−12] have focused on generic water model surfaces. Some studied systems concerning confined water are water in silica pores (Vycor glass),[13] near platinum[14] or magnetite,[15] and in zirconium,[16] mica,[17] or graphite. The geometry of the confining device has been considered to be planar,[18−22] cylindrical (carbon nanotubes),[23−25] or spherical.[26,27] A review of recent developments in the case of water confined in slab geometry from the computational point of view has been reported by Zangi.[28] From the experimental side, numerous contributions are devoted to solid−water interfaces. References close to the present work are refs 29−31.

Nevertheless, it should be pointed out that despite their importance, few studies have been devoted to the calculation of electrical and dielectric properties of water under confinement.[26,27] In a previous work,[32] we observed that the orientational distribution of water molecules at the graphite interfaces reveals two preferential values: one corresponding to dangling H bonds (nonbonded hydrogen atoms pointing to the surface) and a second one corresponding to molecular OH bonds parallel to the surface. It is expected that those features will have some influence on the dielectric properties of water. To establish a bridge between the dielectric and electrochemical properties, in the first part of the paper we will include a detailed analysis of such properties and their relationship to the electrostatic characteristics of the system.

The second aspect that we will study with detail concerns the microscopic dynamics of water under confinement. Some recent studies, devoted to properties such as translational and rotational diffusion coefficients[11,12,33] or the spectroscopic properties of water molecules under confinement,[34,35] have revealed significant changes in water dynamics because of confinement effects. Here we will focus our attention on both translational diffusion and spectroscopy in order to explore the influence of confinement on such properties in the case of graphite slabs of variable separation.

Technical Details

A series of molecular dynamics simulations of liquid water between two parallel graphite plates (HOPG, highly oriented pyrolytic graphite) separated by a distance d at room temperature ($T = 298$ K) and fixed densities have been performed. In every case, the densities are the corresponding values of stable states at each separation at zero pressure. Those stable states were

* Corresponding author. E-mail: jordi.marti@upc.edu.
† Departament de Física i Enginyeria Nuclear.
‡ Materials Department, KFKI-Atomic Energy Research Institute.
§ Departamento de Sistemas Físicos, Químicos y Naturales.

10.1021/jp0647277 CCC: $33.50
Published on Web 11/09/2006

TABLE 1: Simulated Stable States and Cutoff Values for Selected Regions[a] of Water Confined in Graphite Nanochannels

d (nm)	density (g/cm^3)	adsorbed region (nm)	intermediate region (nm)	central region (nm)
0.7	2.89	0.25−0.45		
0.9	0.34	0.27−0.62		
0.9	1.78	0.25−0.65		
1.2	1.65	0.25−0.45, 0.75−0.95		0.45−0.75
1.5	1.18	0.25−0.5, 1.0−1.25		0.5−1.0
3.1	1.04	0.26−0.48, 2.62−2.84	0.48−0.75, 2.35−2.62	0.75−2.35

[a] *Adsorbed* for water nearest the graphite walls, *central* for water in the internal bulklike regions and *intermediate* for the region between the two former ones.

determined in two previous works[22,32] and are specified in Table 1. Densities were computed with consideration only for the available space to water molecules; i.e., the excluded volume due to the influence of graphite walls was subtracted. We set up our simulation box to $3.44 \times 3.41 \times z$ nm^3. These values correspond to the geometry of HOPG in the real systems. The coordinate z corresponds to the interface−interface direction Z. Finally, we defined three different groups of water molecules directly related by their locations with respect to the graphite walls: *adsorbed* for water in the closest layer, *central* for water far from the graphite, and, in the case of $d = 3.1$ nm, an *intermediate* region. The exact definition of those regions in each case comes from the corresponding density profiles,[22,32] and it is reported in Table 1.

Water−water inter- and intramolecular interactions have been modeled with a flexible simple-point-charged (SPC) potential which was specifically reparametrized to reproduce the main trends of the infrared spectrum of water at ambient conditions.[36] Water−carbon forces have been assumed to be of the Lennard-Jones type with the same parametrization employed in previous studies of water near graphite (see ref 37 for instance). Periodic boundary conditions in the X and Y directions have been assumed. Long-range electrostatic interactions have been accounted for by a 3D Ewald sum procedure (see refs 32 and 38 for details). Such a method is based on the increasing length z of the simulation box outside the slab region, leaving enough room for the decoupling of interactions between real and image charges. A leapfrog Verlet integration algorithm with coupling to a thermal bath has also been adopted.[39] Our integration time-step was 0.5 fs. Stabilization runs of more than 50 ps followed by production runs of lengths between 50 and 500 ps were considered in all cases.

In a previous work[32] we analyzed the reliability of the model and procedure employed, comparing our findings with experimental STM (scanning tunneling microscopy) data. We considered the probability of electron transmittance in one dimension between HOPG and a dimensionless imaginary tip, placed at regularly spaced distances from the surface. At the qualitative level, the results from computer simulations and experiments are in good agreement.

Results

Electrostatic Potential Profile. We focused our study of the electric properties of confined water on the analysis of the electrostatic potential profile of water along the available confined space. The electrostatic potential was calculated as a one-dimensional average perpendicular to the graphite surfaces.

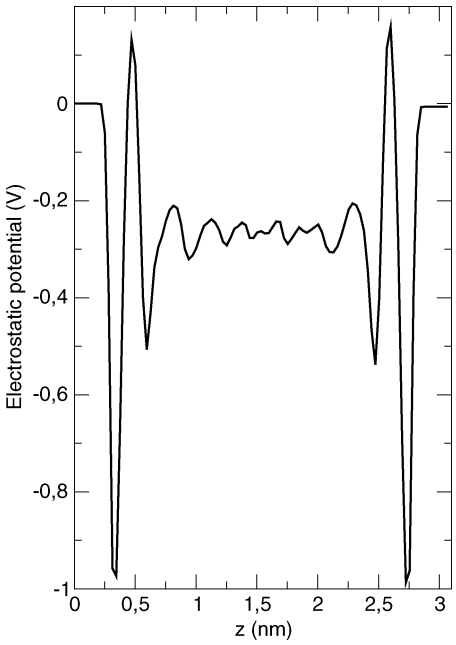

Figure 1. Electrostatic potential profile for $d = 3.1$ nm.

The Poisson equation was solved by taking the charge density of water into account.[40] The results are presented in Figure 1. The potential difference between the HOPG surface and the water bulk, i.e., the surface potential drop, is about −0.28 V. As a comparison, this value is about +0.86 V over that of the Pt(100)−water system,[41] showing that the potential of zero charge is largely different for hydrophobic and hydrophilic surfaces. The electrostatic potential reveals strong fluctuations near the graphite walls and much weaker ones in the intermediate region, and as expected, it is almost constant in the bulk. Our results are in good overall agreement with those of others.[27] The spatial fluctuations in the electrostatic potential are deeply connected with the charge distribution of water in the system (graphite walls are uncharged), since they are calculated from it via the Poisson equation. The resulting profile of the electrostatic potential is very homogeneous in the central region, but it shows a certain degree of ordering in the interfaces because of the preferential orientations of water.[32] This fact will be an indication of large deviations in the dielectric constant compared with the value of unconstrained liquid water, as we will show below.

Dielectric Properties of Water. The dielectric properties of a liquid under confinement may be directly characterized by the calculation of the static dielectric constant ϵ and by means of the analysis of the total dipole moment. In the case of a system with long-range interactions treated by the Ewald method with conducting boundary conditions, the static dielectric constant ϵ is given by[42,43]

$$\epsilon = 1 + \frac{4\pi N\langle\mu^2\rangle G_k}{3Vk_BT} \tag{1}$$

where N is the number of water molecules, V is the accessible volume, $\vec{\mu}(t)$ is the molecular dipole moment of water, k_B is the Boltzmann constant, and G_k is the so-called finite system Kirkwood G factor

$$G_k = \frac{\langle M^2\rangle}{N\langle\mu^2\rangle} \tag{2}$$

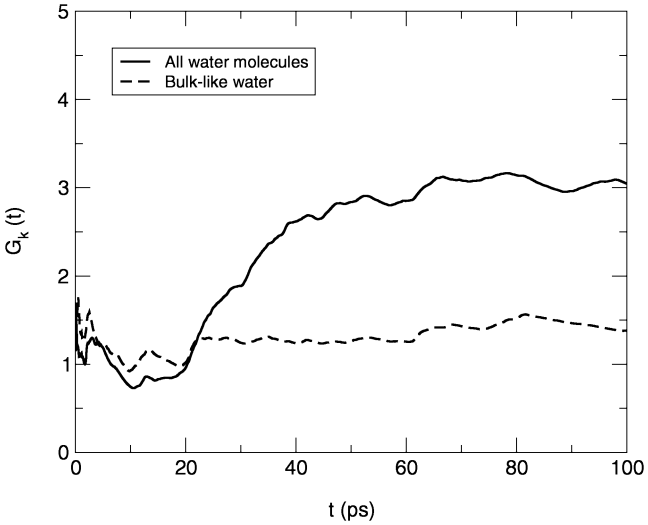

Figure 2. Cumulative average of the Kirkwood *G* factor as a function of the simulation length for $d = 1.5$ nm.

TABLE 2: Dielectric Properties of Water Confined in a Graphite Nanochannel of $d = 3.1$ nm[a]

zone	molecules (%)	G_k	ϵ	C (μF/cm^2)	τ_M (ps)
adsorbed	22.8	6.3	172 ± 95	630.9	25.1
intermediate	17.0	1.5	30 ± 8	109.8	3.4
central	60.2	1.6	35 ± 5	18.7	7.1
total	100	3.9	85 ± 25	28.5	21.8
bulk (unconfined)[44]		3.2	66 ± 2		5.0
experimental[45]			80		9.3

[a]The percentages of water molecules located in the different regions are included. Equivalent capacitances per normal surface unit are also given. Experimental values correspond with those of unconstrained bulk water.

TABLE 3: Dielectric Properties of Water Confined in Graphite Channels of Variable Separation ($d \leq 1.5$ nm)

zone	d (nm)	ϵ	C (μF/cm^2)	τ_M (ps)
adsorbed	0.7	71 ± 3	314.3	350
	0.9 (low density)	3.5 ± 0.2	8.9	5.6
	0.9 (high density)	98 ± 9	216.9	21
central	1.2	51 ± 2	150.5	6.8
	1.5	29 ± 2	51.4	6.8
total	1.2	232 ± 2	293.4	42
	1.5	71 ± 5	62.9	25

being $\vec{M}(t) = \sum_{i=1}^{N} \vec{\mu}_i(t)$ the total dipole moment of the system. Here $\langle ... \rangle$ indicates a statistical average over different configurations.

The results are summarized in Table 2 for the widest case ($d = 3.1$ nm) and in Table 3 for the remaining separations ($d \leq 1.5$ nm). We present the cumulative $G_k(t)$ in Figure 2 for $d = 1.5$ nm as an example of the different behavior of this property for water molecules in the central zone and for all molecules of the system, providing an indication of the influence of confinement in the graphite slab on the dielectric constant of water. In all simulations, the averaged molecular dipole moment $\langle \mu \rangle$ is nearly constant ($\sim$2.46 D). Comparing this to the value obtained for unconfined liquid water with the same model (2.44 D),[46] we see that the difference is negligible.

The values of the Kirkwood *G* factor near the interfaces, i.e., for water molecules located in the adsorbed and intermediate layers showed, in general, large fluctuations and so do the dielectric constants. This is reflected in the estimated errors (Tables 2 and 3). Such errors are especially large in the case of $d = 3.1$ nm. We think that the values that are really meaningful are the ones obtained for the central and total water sets. At this point, we have to note the abnormally large value of ϵ for the full system in the case of $d = 1.2$ nm, which probably should be attributed to the strong orientational order of water here, in agreement with the density profile reported in Figure 6 of ref 22.

The common fact in all cases is that G_k in the central zone for all distances is remarkably lower than the corresponding value for all molecules in the system. In other words, the existence of interfaces due to confinement produces the increase of the global dielectric constant of water. This is in agreement with the fact that the values obtained in the adsorbed layers are in general larger than those from central regions. As indicated above, we tend to think that this can be attributed to the existence of preferential orientations of water when it approaches the interfaces (see ref 32 for details). Such orientations would favor larger values of dipole−dipole correlations and, consequently, explain the large ϵ observed. Interestingly, this is in good agreement with the findings of Ballenegger and Hansen[27] for slab and spherical geometries, who observed the increase of the dielectric constant when moving from bulklike regions to the interfaces. Nevertheless, other authors such as Senapati and Chandra[26] obtained a systematic reduction of ϵ for water confined in spherical nanocavities as the cavity diameter was reduced. However, it should be pointed out that their biggest cavity size (with a diameter of 2.44 nm) is the one producing the largest values of ϵ (between 60 and 70), whereas the nanochannel of separation $d = 3.1$ nm considered in the present work produced a value of 85 (Table 2) that should be compared with the ϵ obtained for water in a spherical cavity of similar size.

When the characteristics of the surface are considered, we should compare our findings with those obtained for hydrophilic surfaces, such as platinum.[40] In that case, the presence of platinum walls reduced the value of the dielectric constant of bulk confined water (central part of the system) to an estimated value of 55, clearly smaller than the experimental result for bulk unconstrained water (around 80). This fact is qualitatively similar to our findings: our reported value for the dielectric constant in the central "bulklike" region is 35, i.e., smaller than the experimental bulk unconfined value as well. The explanation of this feature given by Nagy and Heinzinger[40] consisted in assuming the Kirkwood-Booth theory which indicates that a saturation effect produced by high electric fields is responsible for the reduction of the dielectric constant in the central region.

An additional discussion is about the role of water as a dielectric substance, able to screen the influence of external electric fields. We assumed an ideal capacitor as a "test" system. In this way, we included in Table 2 an estimation of the capacitance per surface unit *C* of a flat capacitor of surface $S = 3.44 \times 3.41$ nm ^{2} parallel to the graphite walls and containing our simulation sets. We computed the results for such a parameter in all regions of the system. Here, capacitance is simply computed as $C = \epsilon_0 \epsilon S/d$. The general trend is the good qualitative agreement of overall values (on the order of 10−100 μF/cm^2) within the typical magnitudes of capacitance of interfaces in aqueous electrochemical systems (see ref 47). The main fact observed in the reference system of wide separation ($d = 3.1$ nm) is the large value of *C* at interfaces, compared to the average value and to *C* at the central part of the system. For highly confined systems ($d = 0.7$, 0.9 nm), capacitances are similar to those of adsorbed water in the former case, since now the central bulklike part, which helps to reduce the overall value in the wider systems, is simply absent. The only

TABLE 4: Residence Times of Water for $d = 1.2$, 1.5, 3.1 nm, and Diffusion Coefficients[a] of Oxygen Atoms in the Z Direction, along the XY Plane, and Overall Values

zone	d (nm)	τ_{res}^{I} (ps)	τ_{res}^{C} (ps)	D	D_{XY}	D_Z
adsorbed	0.7			1.0	1.5	~0
	0.9 (low density)			6.5	9.7	0.2
	0.9 (high density)			1.1	1.7	~0
	1.2	352	81.8	1.8	2.7	0.03
	1.5	58.4	13.4	2.7	3.9	0.3
	3.1	54.0	12.0	3.7	5.3	0.3
intermediate	3.1	14.0	2.8	3.6	5.1	0.6
central	1.2	170.4	91.0	1.9	2.8	0.07
	1.5	42.9	17.8	3.0	4.3	0.5
	3.1	127.0	57.5	3.5	4.9	0.8

[a] Expressed in 10^{-5} cm^2/s.

remarkable difference corresponds to the case of low density for $d = 0.9$ nm, where the low value of ϵ (probably due to the existence of large cavities in the system, allowing loss of correlation of molecular dipole moments) is the main reason of this effect. Intermediate cases such as those at separations of 1.2 and 1.5 nm produce values of C in the middle range of the two extreme cases cited above.

As dynamical dielectric properties associated with the total and molecular dipole moments, the relaxation times of total (τ_M) and molecular (τ_μ) dipole moments are computed as

$$\tau_M = < \int_0^\infty \frac{\langle \vec{M}(t)\cdot\vec{M}(0)\rangle}{\langle M^2(0)\rangle} dt$$

$$\tau_\mu = \int_0^\infty \frac{\langle \vec{u}_\mu(t)\cdot\vec{u}_\mu(0)\rangle}{\langle \mu^2(0)\rangle} dt \qquad (3)$$

Our results for τ_M are included in Tables 2 and 3. In this section, we will only discuss the main features of τ_M, leaving the discussion on τ_μ to the section on "reorientational times". Here, we just would like to point out that the largest deviations from the experimental value observed in τ_M are basically due to interfacial effects, in such a way that we get a value of 350 ps in the case of $d = 0.7$ nm. This indicates that dipole moments remain oriented along fixed directions for long times. This effect seems to be milder as the slab separation increases, although we still can observe long relaxation times for τ_M in the rest of the graphite−graphite separations ($d = 1.2$, 1.5, 3.1 nm).

Residence Times of Water Molecules. The residence times of water molecules in their first coordination shells may be defined as the mean time that a water molecule spends in its hydration shell before it moves away to coordination shells of higher order. We can directly define two of those times τ_{res}^{I} and τ_{res}^{C} in the way described by Impey et al.[48] The I superscript indicates the "intermittent" character of the computed time; i.e., we allow the multiple re-entrance of water molecules until they definitely leave the given region for a time period of "infinite" length. For practical purposes, such infinite length in time is taken to be of the order of a nanosecond. Conversely, the C superscript indicates the "continuous" residence time, i.e., computed until a water molecule leaves the region for the first time.

We collected the values of residence times of water molecules in each region of the system in Table 4 for separations $d \leq 1.5$ nm. The results for the widest case of $d = 3.1$ nm were reported in a preliminary work[32] and have been added for comparison. The general trend is, as expected, that the intermittent values are much larger than continuous ones. In the same way as for the 3.1 nm slab, the largest differences arise in the case of adsorbed water. We note that the values for bulk water are larger than those of adsorbed and intermediate water, with the exception of the intermittent time for $d = 1.2$ nm. Water at the interfaces is very stable (with extremely large, i.e., on the order of a nanosecond, values for the residence times of water in the narrow separations of 0.7 and 0.9 nm, which have not been reported). A general trend is that the smaller the separation d, the longer both τ. However, it has to be remembered that the density profiles of water along such narrow systems (see ref 22) indicate the existence of "central" water layers that cannot be considered similar to "bulk" water since they are strongly influenced by the presence of the graphite walls. Furthermore, noting the persistence of water molecules in each region is relevant to the meaningfulness of the calculation of other dynamical quantities such as relaxation and reorientational times, transport coefficients, and spectral densities. So, once the reliability of the computation of dynamical properties had been established, we proceeded with the analysis in the following sections.

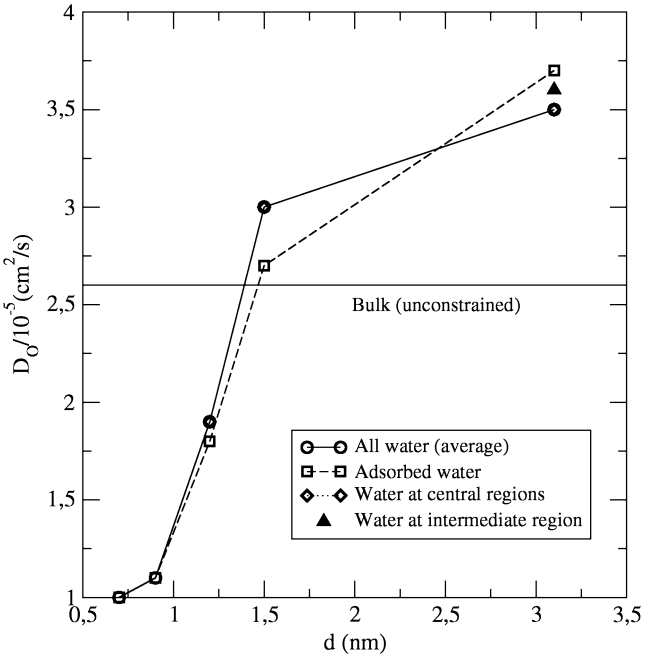

Figure 3. Diffusion coefficients of oxygens for several graphite−graphite distances.

Self-Diffusion Coefficients. The diffusive behavior of water under confinement has been found to be significantly different than that of the unconstrained liquid.[12,49] In this work we report the self-diffusion coefficients of water for five distances between the graphite slabs. We considered the diffusion D_O of oxygen atoms, since the center of mass of the whole water molecule is roughly located in the oxygen site. We computed D by means of the time integration of the oxygen velocity autocorrelation functions or, equivalently, as the long time slope of the mean square displacement of oxygen atoms. We distinguished between water molecules located in each of the different locations, basically the adsorbed layers and central regions. In the case of the widest graphite−graphite separation $d = 3.1$ nm, we have also considered the diffusion of water molecules located in the intermediate zone between the adsorbed layers and the central area. Furthermore, we also computed the diffusion coefficients along the Z direction by considering the projections of atomic velocities and positions on the z coordinate.

The results are presented in Figure 3 and Table 4 and compared with the diffusion coefficient of oxygens in uncon-

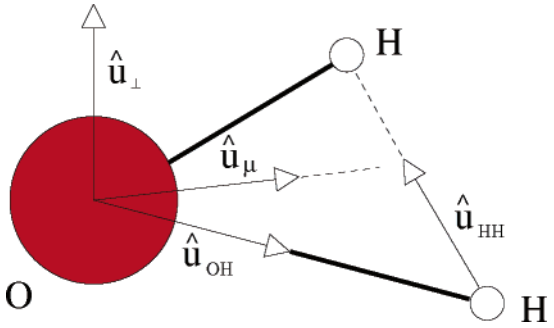

Figure 4. Unit vectors along selected molecular directions.

strained liquid water at 298 K (2.6×10^{-5} cm^2/s). At first sight, we can observe that the diffusion coefficients of confined water are generally smaller than their bulk unconstrained water counterparts. This is in good overall agreement with the findings obtained by Liu et al.[50] using the TIP3P model.

Two other general trends are observed: first, that diffusion is directly related with the graphite−graphite separation distance d, being greater for larger distances but showing linear dependence only for short d separations; and second, that water molecules located in the interfaces diffuse slower than those placed in the internal bulklike regions. The first result is, in our opinion, directly connected with the extent of space available in each case, in such a way that the systems with water placed at short graphite−graphite separations (especially $d = 0.7$, 0.9 nm) are able to pack water molecules very strongly, leaving basically no room for translational motions. From the microscopic point of view, low values of D are connected to molecular motions in restricted areas. Nevertheless, it is interesting to note that for the $d > 1.5$ nm separations, D is larger than the values obtained for unconstrained water. In those particular cases, a large percentage of water is far from the interfaces, and consequently the influence of the walls is reduced, producing values of D close to those of unconstrained water.

With regard to more specific features, we should state that: (1) the only case with an intermediate region ($d = 3.1$ nm) produced a value of D in the range of 3.5×10^{-5} cm^2/s, very similar to the values of bulk water; and (2) the calculation of the Z direction diffusion coefficients for $d = 3.1$ nm reported values of 0.3×10^{-5} cm^2/s in the interfaces, 0.6×10^{-5} cm^2/s in the intermediate region, and 0.8×10^{-5} cm^2/s in the bulklike region. This latter fact indicates that diffusion in confined water is mainly due to molecular motions along planes parallel to the surfaces. In the case of close separations between slabs, the diffusion along the Z direction is extremely low, on the order of diffusion in solids, in the same fashion as it has been observed at high temperatures.[51]

Reorientational Times of Water Molecules. The structural orientational order of water at interfaces was previously studied.[32] In this work, we focus our attention on the dynamics of the orientational properties of water. This can be analyzed by means of a series of time correlation functions $C_{l,\alpha}(t)$ defined as follows

$$C_{l,\alpha}(t) \equiv \langle P_l(\hat{u}_\alpha(t)\cdot\hat{u}_\alpha(0))\rangle \qquad (l = 1, 2) \tag{4}$$

where P_l is the lth Legendre polynomial and $\hat{u}_\alpha$ is a unit vector along a given molecular direction. We considered only the case of $l = 1$ and four unit vectors: $\hat{u}_\mu$ defined along the molecular dipole moment direction, $\hat{u}_{OH}$ and $\hat{u}_{HH}$ along the O−H and H−H directions, and $\hat{u}_\perp \equiv \hat{u}_\mu \times \hat{u}_{HH}$. The latter is perpendicular to the instantaneous molecular plane (see Figure 4). As an example, we show in Figure 5 a comparison of the four correlation

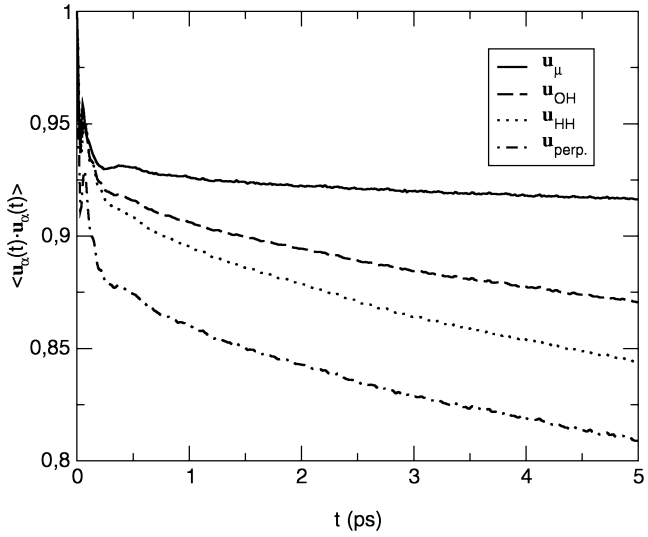

Figure 5. Time correlation functions of several reorientational times at the graphite−graphite separation of $d = 0.7$ nm.

TABLE 5: Reorientational Times along Selected Directions of Water Molecules Confined in Graphite Nanochannels

zone	d (nm)	$\tau_{\vec{\mu}}$ (ps)	$\tau_{\vec{OH}}$ (ps)	$\tau_{\vec{HH}}$	$\tau_{\perp}$	τ_M/τ_μ
	0.7	405	99.5	66	63	0.9
	0.9 (low density)	5.6	3.5	2.6	2.3	1.0
adsorbed	0.9 (high density)	15.1	10.8	9.0	7.8	1.4
	1.2	16.0	11.3	9.5	8.4	
	1.5	8.3	5.8	4.7	4.0	
	3.1	8.7	5.6	4.6	4.0	2.9
intermediate	3.1	5.1	4.2	3.8	2.7	0.7
	1.2	5.8	4.2	3.5	2.7	1.2
central	1.5	4.9	4.4	4.1	2.9	1.4
	3.1	5.1	4.7	4.5	3.1	1.4
	1.2	11.0				3.8
total	1.5	6.5				3.8
	3.1	5.6				3.9
bulk (unconstrained)[53]		4.9		4.3	3.1	1.0
experimental[45]		3.6				2.6

functions $C_{1,\alpha}(t)$ for the case of $d = 0.7$ nm. From $C_{1,\alpha}(t)$ we can compute the so-called *characteristic reorientational times* (τ_α) along each selected molecular direction

$$\tau_\alpha = \int_0^\infty \mathrm{d}t\, C_{1,\alpha}(t) \tag{5}$$

These times give an indication of the mean time employed by a given molecular direction (that of the dipole moment, of the O−H and H−H directions, or the instantaneous direction perpendicular to the molecular plane) to significantly change its orientation in time. To be more precise, it is known that $C_{1,\mu}(t)$ can be related with dielectric relaxation measurements[52] whereas other correlation functions (not considered here) such as $C_{2,OH}(t)$ and $C_{2,HH}(t)$ are connected to nuclear magnetic resonance experiments.

Our results are presented in Table 5 for all separations considered in the present work. Almost all values are of the order of magnitude of those obtained in unconstrained bulk water simulations, i.e., between 3 and 5 ps. Not surprisingly, the results on the central regions are basically equal to those of bulk water, with few τ sensitive to changes in the slab separation, except for the case of adsorbed water, when all reorientational times rise up to higher values. The most remarkable changes arise when we consider the strongest confinement, for $d = 0.7$ nm. In this particular case, water shows huge reorientational

times (a trend that was already observed for residence times), so changes along all defined axes are extremely slow. As a secondary general trend, we observed qualitatively similar behavior of water reorientation as a function of the spatial direction, i.e., there is a tendency to isotropy in all cases. It should be pointed out that in the case of hydrophilic surfaces such as platinum,[54] the relaxation times of the molecular dipole moment were found to be of around 3 ps in bulklike regions and to increase to about 8 ps for the adsorbed water layers. Remarkably, the trends and values reported in this study are very similar.

A closer look at τ_μ reveals that it is markedly affected only in the case of adsorbed water, basically due to the extra ordering induced by the graphite walls in their closest molecules. In the other cases its value is very close to 5. The ratio τ_M/τ_μ gives an indication of the weight of cross correlations in the reorientations of the dipole moment,[43,55] the value being close to 1 for ideal gases and deviating from such value as the system approaches the characteristics of a liquid. In the case of $d = 3.1$ nm, we again observe that the value for the total system is larger than the value for the central part, giving an indication of the influence of water located close to the graphite slabs. The value for the unconfined bulk liquid is close to the latter but somewhat lower than the experimental one. This fact indicates that the model used in this work tends to underemphasize the role of crossed terms in the total dipole moment autocorrelation function. For systems where the separations between the graphite slabs are smaller, $d \leq 1.5$ nm, we found huge values of τ_μ in the case of $d = 0.7$ nm and relaxation times typically large for adsorbed water at interfaces, of about 2 or 3 times those of central regions. This is directly seen in the case of $d = 0.9$ nm at high density and indirectly observed by comparison of values from total and central regions ($d = 1.2$, 1.5 nm). The only case with smaller relaxation times is for $d = 0.9$ nm and low density, where water molecules have some additional room to move and rotate, allowing longer τ. We observed that the ratio τ_M/τ_μ is close to 1 at interfaces and that it increases in the central regions, where the influence of the walls is milder.

Molecular Spectroscopy. Microscopic dynamics of liquids is usually studied from the experimental side by means of molecular spectroscopy measurements. In this work we will present a series of spectral densities which can be directly compared with infrared or Raman data,[44] at least concerning the location of the spectral bands. To do this, we computed spectral densities $S(\omega)$ through the Fourier transforms of the hydrogen and oxygen velocity autocorrelation functions $\langle \vec{v}(t)\cdot\vec{v}(0)\rangle$, following a standard procedure already employed in previous works (see ref 44).

The results for short distance slab separations are included in Figures 6 and 7 and those for long distances are displayed in Figures 6 and 8. In the case of spectral densities of hydrogens (Figure 7), the full spectral range has been separated into three parts: rotational motions $S_R(\omega)$, bending vibrations $S_B(\omega)$, and stretching vibrations $S_S(\omega)$.

In the low-frequency region (0−400 cm^{-1}), two main bands are observed in the experimental spectra (see ref 56 for a discussion about their physical meaning), one around 50 cm^{-1} (band A), associated with restricted translations of water inside the cage of neighboring molecules, and a second band located around 200 cm^{-1} (band B), which can be regarded as the signature of hydrogen-bond stretching vibrations. The details must be investigated from Figure 6, where oxygen spectral densities are presented, since those low-frequency motions are mainly due to the slow vibrations undertaken by oxygens. At

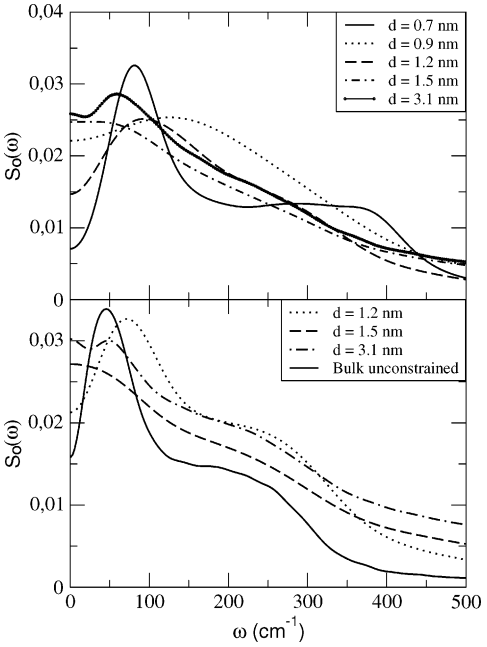

Figure 6. Spectral densities of oxygens for adsorbed water (top) and in central regions (bottom) for several graphite−graphite distances. The case of $d = 0.9$ nm corresponds to the high-density case.

low graphite−graphite separations (top of Figure 6), we observe that band A is blue-shifted by 50−100 cm^{-1} in the more packed systems (0.7 and 0.9 nm high density separations). This indicates that extreme packing tends to produce restricted translations of water at higher frequencies. In the case of wide graphite−graphite separations (bottom of Figure 6), the tendency is to converge to the value of unconstrained bulk (50 cm^{-1}). Concerning band B, only for the case of $d = 0.7$ nm a significant spectral shift (the band is centered close to 400 cm^{-1}) is obtained. This is in reasonable agreement with the idea to assign this band to hydrogen-bond stretching vibrations, which are basically local motions that should not be very affected by confinement effects. However, when confinement is forcing water to have a quasi-two-dimensional structure (i.e., for $d = 0.7$ nm) instead of the usual tetrahedral ordering in bulk water, such vibrations are dramatically affected. In our opinion, this is surely related to the stronger interactions between water and the graphite walls, which would be responsible for higher frequency vibrations. Furthermore, the comparison of our results with those from Choudhury and Pettitt,[12] who used the rigid SPC/E model, indicates an excellent agreement for the case of $d = 0.7$ nm (which roughly corresponds to 0.68 nm in ref 12): a single band centered around 80 cm^{-1} is observed in both works.

High-frequency vibrations are analyzed in Figures 7 and 8. In Figure 7 we explored the cases of the narrowest graphite−graphite separations ($d \leq 0.9$ nm), compared with the corresponding spectral density of hydrogens of adsorbed water at $d = 3.1$ nm. The differences between the adsorbed and central region water are reported in Figure 8 by means of the spectral densities $S_A(\omega)$ and $S_C(\omega)$, respectively. Here we only considered large values of d ($d \geq 1.2$ nm), since only in those cases can we clearly observe distinct adsorbed and central water molecules. In all cases, the spectral shifts will be defined as the differences of the maxima of spectral bands with respect to the corresponding maxima in the bulk system.

The range between 300 and 900 cm^{-1} corresponds to rotational motions of the instantaneous molecular plane and reveals (Figure 6) slight displacements of the central band

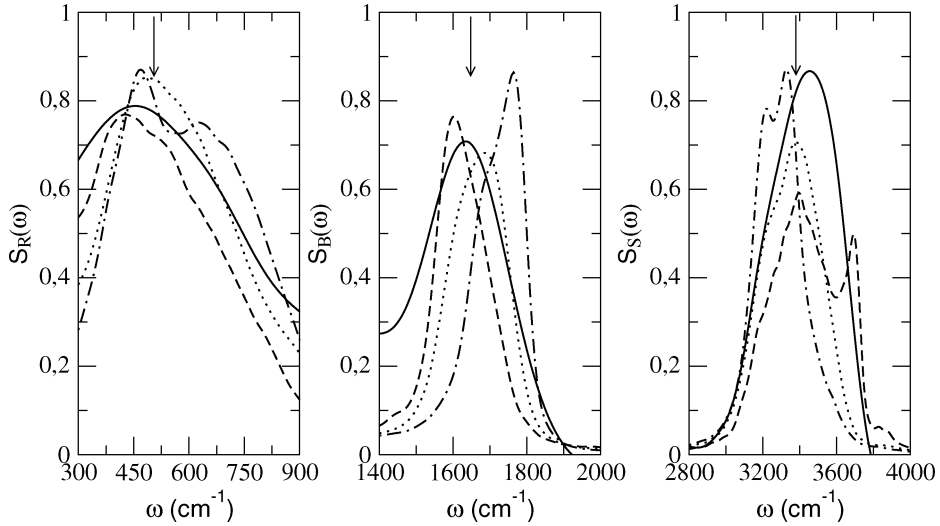

Figure 7. Spectral densities of hydrogens for adsorbed water at slab separations of $d = 0.7$ nm (dot-dashed line), $d = 0.9$ nm at low density (dashed line), and $d = 0.9$ nm at high density (dotted line). For the sake of comparison, we included the spectrum of adsorbed water at $d = 3.1$ nm (solid line). The arrows indicate the maxima of each spectral band in the case of bulk unconstrained water.[57]

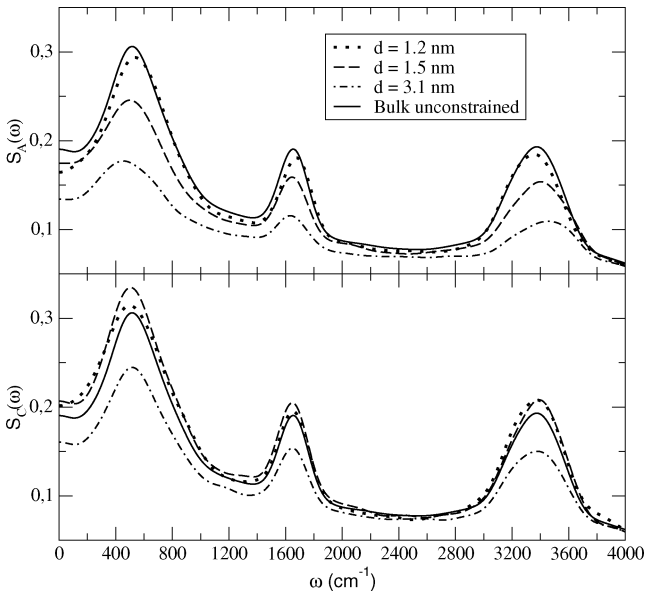

Figure 8. Spectral densities of hydrogens for adsorbed water ($S_A(\omega)$) and in central regions ($S_C(\omega)$) for $d \geq 1.2$ nm.

(located at 505 cm^{-1} in bulk unconstrained water[57]). The new facts are as follows: (1) The displacement of this band to ~420 cm^{-1} in the case of $d = 0.9$ nm at low density. This could be related to the slow librations typical of gases, since the structure of water in this particular case includes large regions where water is surrounded by vacuum areas (see ref 32). (2) The appearance of a new peak around 650 cm^{-1} for the narrowest separation of 0.7 nm has to be clearly attributed to a confinement effect which would involve faster rotations along the *XY* plane. For this librational band, no significant differences are seen in the case of wide ($d > 0.9$ nm) separations when spectra from water located at the adsorbed and central regions are compared (Figure 7).

In the bending region (1400−1900 cm^{-1}), the most relevant feature is the blue-shift in the spectra of highly packed water systems ($d = 0.7$ nm and $d = 0.9$ nm at high density) when compared with the spectrum of the widest $d = 3.1$ nm slab. However, in the case of $d = 0.9$ nm at low density there is no clear shift. We tend to believe that extremely confining slabs force water to internally vibrate at higher frequencies (most remarkable in the case of extreme packing, $d = 0.7$ nm), whereas systems at low density tend to have bending frequencies closer to the gas-phase values (1 594 cm^{-1} for unconstrained water[58]). For large separations ($d > 0.9$ nm), no significant differences are found between the frequencies of the bending motions of bulk and interfacial water.

Finally, in the stretching region (2800−4000 cm^{-1}) we again found relevant changes in the cases of low distances ($d < 0.9$ nm) and low density ($d = 0.9$ nm, 0.0047 g/cm^3). Now we observe the red-shift of maxima of spectral bands in the highly packed systems with respect to the value of our reference system, i.e., for $d = 3.1$ nm. Another new fact is the tendency of interfacial water (especially for $d = 3.1$ nm) to blue-shifting (top of Figure 8). It is difficult to explain this effect using simple arguments, but we believe that two factors are playing a role: on one hand the size of the adsorbed region, and on the other hand the interactions with the walls and the surroundings (internal water).

For low d (Figure 6), a small displacement to lower frequencies is observed for water at extreme confinement ($d = 0.7$ nm), and the splitting of the stretching band into two parts is found for the particular case of $d = 0.9$ nm, 0.0047 g/cm^3. This latter fact is, in our opinion, due to the increase in the number of water molecules with nonbonded hydrogens, taking place in a similar fashion to what happens in other highly constrained systems, such as water inside carbon nanotubes.[34] This is in good agreement with the facts that (1) such particular case includes large vacuum-interface regions and (2) stretching of water at the gas-phase happens at higher frequencies (3650−3750 cm^{-1}) than in liquid ambients.[58]

Concluding Remarks

Molecular dynamics simulation has been applied to the calculation of electrostatic, dielectric, and dynamical properties of liquid water constrained by graphite slabs at variable separation. We observed an overall surface potential drop of −0.28 V in the electrostatic potential profile, this being almost 1 V smaller than in the case of a typical hydrophilic metal surface such as Pt(100). Fluctuating electrostatic interactions are stronger in molecules that are closer to the interfaces. An increase of the dielectric constant is observed when the interfaces are approached from the central bulklike regions. We think that

this effect has to be attributed to the better ordering of water in the interfaces, where two preferential orientations were found. Such larger ordering degree would induce the existence of stronger correlations between molecular dipole moments, and in consequence, they would be responsible for the larger values of ϵ.

Concerning residence and reorientational times of water molecules in the different regions, there is a general trend which basically consists of the slowing down of molecular motions as the systems decrease in size (or accessible volume) and as water molecules are closer to interfaces, with some marked cases such as those of strongest confinement (especially for $d = 0.7$ nm), where the severe packing and ordering of water suggests long-lived configurations and typical regimes for reorientations on the order of a nanosecond.

The diffusive behavior of water is affected by confinement, in line with the results obtained for water confined inside carbon nanotubes.[49] Here, we found a dramatic reduction in the self-diffusion coefficient of water in the case of the narrowest graphite−graphite distances ($d \leq 0.9$ nm) compared with the typical values of bulk water and values close to the experimental bulk value[59] (about 2.3×10^{-5} cm^2/s) for all the wider separations. In the particular case of $d = 3.1$ nm, the diffusion is close to the value of bulk unconstrained water, which indicates that the extent of space available is the key factor in diffusion, far more important that the water−surface interaction, at least for hydrophobic walls.

Spectroscopy has been considered the means of the computation of power spectra of oxygen and hydrogen atoms. In summary, we observed marked spectral shifts in the cases of high confinement, i.e., for the lowest graphite−graphite distances. In those cases, we expect that such displacements of spectral bands might be detected by appropriate infrared spectrum measurements in the way that the infrared spectra of low-temperature (92 K) water has recently been studied.[60]

Acknowledgment. G.N. is indebted for the financial support of the National Science Research Fund, Hungary (OTKA) under Contract No. T049202. M.C.G. and J.M. gratefully acknowledge financial support from the Direcció General de Recerca de la Generalitat de Catalunya (Grant 2005SGR-00779) and the Ministerio de Educación y Ciencia of Spain (Grant BFM2003-08211-C03-01). Financial support of the Grupo FQM-215 of Plan Andaluz de Investigación (PAI) and a joint Spain−Hungary Integrated Action with references E−36/04 (Hungary) and HH2004-0006 (Spain) are also acknowledged, as well as funds from the European Union (FEDER, Ref. UNPC-E015).

References and Notes

(1) Gileadi, E.; Kirowa-Eisner, E.; Penciner, J. *Interfacial Electrochemistry*; Addison-Wesley: Reading, MA, 1975.
(2) Thiel, P. A.; Madey, T. E. *Surf. Sci. Rep.* **1987**, *7*, 211.
(3) Bartón, K. *Protection Against Atmospheric Corrosion: Theories and Methods*; Wiley: London, 1976.
(4) Butler, G.; Ison, H. C. K. *Corrosion and Its Prevention in Waters*; Reinhold: New York, 1966.
(5) Butler, J. R. *Sep. Sci. Technol.* **1980**, *15*, 371.
(6) Don, J. A.; Scholten, J. J. F. *Faraday Discuss. Chem. Soc.* **1971**, *71*, 145.
(7) Turner, J. E.; Hendewerk, M.; Somorjai, G. A. *Chem. Phys. Lett.* **1984**, *105*, 581.
(8) Lee, C. Y.; McCammon, J. A.; Rossky, P. J. *J. Chem. Phys.* **1984**, *80*, 4448.
(9) Zhu, S.-B.; Robinson, G. W. *J. Chem. Phys.* **1990**, *94*, 1403.
(10) Mamatkulov, S. I.; Khabibullaev, P. K.; Netz, R. R. *Langmuir* **2004**, *20*, 4756.
(11) Choudhury, N.; Pettitt, B. M. *J. Am. Chem. Soc.* **2004**, *127*, 3556.
(12) Choudhury, N.; Pettitt, B. M. *J. Phys. Chem. B* **2005**, *109*, 6422.
(13) Rovere, M.; Ricci, M. A.; Vellati, D.; Bruni, F. *J. Chem. Phys.* **1998**, *108*, 9859.
(14) Spohr, E. *Chem. Phys.* **1990**, *141*, 87.
(15) Rustad, J. R.; Felmy, A. R.; Bylaska, E. J. *Geochim. Cosmochim. Acta* **2003**, *67*, 1001.
(16) Martins, L. R.; Skaf, M. S.; Ladanyi, B. M. *J. Phys. Chem. B* **2004**, *108*, 19687.
(17) Leng, Y.; Cummings, P. T. *Phys. Rev. Lett.* **1993**, *70*, 2313.
(18) Gordillo, M. C.; Martí, J. *J. Chem. Phys.* **2002**, *117*, 3425.
(19) Striolo, A.; Chialvo, A.; Cummings, P. T.; Gubbins, K. E. *Langmuir* **2003**, *19*, 8583.
(20) Cabrera Sanfelix, P.; Holloway, S.; Kolasinski, K. W.; Darling, G. R. *Surf. Sci.* **2003**, 532, 166.
(21) Pertsin, A.; Grunze, M. *J. Phys. Chem. B* **2004**, *108*, 1357.
(22) Gordillo, M. C.; Nagy, G.; Martí, J. *J. Chem. Phys.* **2005**, *123*, 054707.
(23) Hummer, G.; Rasaiah, J. C.; Noworyta, J. P. *Nature* **2001**, *414*, 188.
(24) Gordillo, M. C.; Martí, J. *Phys. Rev. B*: *Condens. Matter Mater. Phys.* **2003**, *67*, 205425.
(25) Striolo, A.; Chialvo, A.; Cummings, P. T.; Gubbins, K. E. *J. Chem. Phys.* **2006**, *124*, 074710.
(26) Senapati, S.; Chandra, A. *J. Phys. Chem. B* **2001**, *105*, 5106.
(27) Ballenegger, V.; Hansen, J.-P. *J. Chem. Phys.* **2005**, *122*, 114711.
(28) Zangi, R. *J. Phys.: Condens. Matter* **2004**, *16*, S5371.
(29) Nagy, G. *J. Electroanal. Chem.* **1996**, *409*, 19.
(30) Ricci, M. A.; Bruni, F.; Gallo, P.; Rovere, M.; Soper, A. K. *J. Phys.: Condens. Matter* **2000**, *12*, A345.
(31) Scodinu, A.; Fourkas, J. T. *J. Phys. Chem. B* **2002**, *106*, 10292.
(32) Martí, J.; Nagy, G.; Gordillo, M. C.; Guàrdia, E. *J. Chem. Phys.* **2006**, *124*, 094703.
(33) Liu, P.; Harder, E.; Berne, B. J. *J. Phys. Chem. B* **2004**, *108*, 6595.
(34) Martí, J.; Gordillo, M. C. *Phys. Rev. B*: *Condens. Matter Mater. Phys.* **2001**, *63*, 165430.
(35) Kolesnikov, A. I.; Zanotti, J.-M.; Loong, C.-K.; Thiyagarajan, P.; Moravsky, A. P.; Loufty, R. O.; Burnham, C. J. *Phys. Rev. Lett.* **2004**, *93*, 035503.
(36) Martí, J.; Padró, J. A.; Guàrdia, E. *J. Mol. Liq.* **1994**, *62*, 17.
(37) Gordillo, M. C.; Martí, J. *Chem. Phys. Lett.* **2000**, *329*, 341.
(38) Spohr, E. *J. Chem. Phys.* **1997**, *107*, 6342.
(39) Berendsen, H. J. C.; Postma, J. P. M.; van Gunsteren, W. F.; DiNola, A.; Haak, J. R. *J. Chem. Phys.* **1984**, *81*, 3684.
(40) Nagy, G.; Heinzinger, K. *J. Electroanal. Chem.* **1990**, *296*, 549.
(41) Nagy, G.; Denuault, G. *J. Electroanal. Chem.* **1997**, *433*, 161.
(42) de Leeuw, S. W.; Perram, J. W.; Smith, E. R. *Proc. R. Soc. London Ser. A* **1983**, *388*, 177.
(43) Guàrdia, E.; Martí, J. *Phys. Rev. E: Stat., Nonlinear, Soft Matter Phys.* **2004**, *69*, 011502.
(44) Martí, J.; Guàrdia, E.; Padró, J. A. *J. Chem. Phys.* **1994**, *101*, 10883.
(45) Neumann, M. *J. Chem. Phys.* **1986**, *85*, 1567.
(46) Martí, J. *J. Chem. Phys.* **1999**, *110*, 6876.
(47) Bard, A. J.; Faulkner, L. R. *Electrochemical Methods. Fundamentals and Applications*; John Wiley and Sons: New York, 2001.
(48) Impey, R. M.; Madden, P. A.; McDonald, I. R. *J. Phys. Chem.* **1983**, *87*, 5071.
(49) Martí, J.; Gordillo, M. C. *J. Chem. Phys.* **2001**, *114*, 10486.
(50) Liu, Y.-C.; Wang, Q.; Lu, L.-H. *Chem. Phys. Lett.* **2003**, *381*, 210.
(51) Gordillo, M. C.; Martí, J., submitted.
(52) Madden, P.; Kivelson, D. *Adv. Chem. Phys.* **1984**, *56*, 467.
(53) Martí, J.; Guàrdia, E.; Gordillo, M. C. *Chem. Phys. Lett.* **2002**, *365*, 536.
(54) Nagy, G.; Heinzinger, K.; Spohr, E. *Faraday Discuss. Chem. Soc.* **1992**, *94*, 307.
(55) Saiz, L.; Guàrdia, E.; Padró, J. A. *J. Chem. Phys.* **2000**, *113*, 2814.
(56) Padró, J. A.; Martí, J. *J. Chem. Phys.* **2004**, *120*, 1659.
(57) Martí, J.; Padró, J. A.; Guàrdia, E. *J. Chem. Phys.* **1996**, *105*, 639.
(58) Chen, S. H.; Toukan, K.; Loong, C. K.; Price, D. L.; Teixeira, J. *Phys. Rev. Lett.* **1984**, *53*, 1360.
(59) Krynicki, K.; Green, C. D.; Sawyer, D. W. *Faraday Discuss. Chem. Soc.* **1978**, *66*, 199.
(60) Bolina, A. S.; Wolff, A. J.; Brown, W. A. *J. Phys. Chem. B* **2005**, *109*, 16836.